Journal of Electroanalytical Chemistry 731 (2014) 172–178

Contents lists available at ScienceDirect

Journal of Electroanalytical Chemistry

journal homepage: www.elsevier.com/locate/jelechem

Graphite–castor oil polyurethane composite electrode surfaces – AFM morphological and electrochemical characterisation

Ana-Maria Chiorcea-Paquim [a], Victor Constantin Diculescu [a], Priscila Cervini [b], Eder Tadeu Gomes Cavalheiro [b], Ana Maria Oliveira Brett [a,*]

[a] Department of Chemistry, University of Coimbra, 3004-535 Coimbra, Portugal
[b] Instituto de Química de São Carlos, Departamento de Físico-Química, Universidade de S. Paulo, Caixa Postal 780, São Carlos, Brazil

ARTICLE INFO

Article history:
Received 21 May 2014
Received in revised form 15 July 2014
Accepted 22 July 2014
Available online 14 August 2014

Keywords:
Graphite
Polyurethane
Composite electrode material
AFM
Voltammetry

ABSTRACT

Graphite–castor oil polyurethane composite electrodes with different graphite weight percentages, 30–70% graphite–polyurethane w w^{-1}, were morphologically studied by atomic force microscopy (AFM) and voltammetry. AFM images and *r.m.s.* roughness measurements demonstrated that the polyurethane roughness decreased with increasing the graphite content, composites of 50% and 60% graphite–polyurethane w w^{-1} showing the smother electrode surface. The electrochemical characterisation was performed in solutions of $K_4Fe(CN)_6$ by cyclic voltammetry and impedance spectroscopy. For compositions of 60% and 70% graphite–polyurethane w w^{-1}, the cyclic voltammetry results showed the $K_4Fe(CN)_6$ system reversibility. The charge transfer resistance, determined from the EIS spectra, decreased significantly with increasing the graphite/polyurethane ratio, and the capacitance increased for higher graphite percentages. AFM and voltammetric results enable to conclude that 60% graphite–polyurethane w w^{-1} was the optimal composition for the preparation of the graphite–polyurethane composite electrodes.

1. Introduction

Carbon, such as glassy carbon, carbon fibers, graphite or carbon black, has received grown interest as electrode material because it exhibits several unique properties, including good electrical conductivity, chemical inertness and wide electrochemical potential window, particularly in the positive range, being used as the conductive phase in composite materials for electrochemical sensors [1,2].

A composite can be defined as a material composed of at least one conducting phase commingled with at least one insulator phase [3], the last acting as an agglutinant. Carbon composite electrodes, obtained by using a mixture of particulate conductive carbon phase and an insulating matrix, represented an attractive approach to the fabrication of electrochemical sensors, whose surface can be renewed by polishing.

Several examples of graphite composite electrodes where described in the literature, being used for amperometric and voltammetric determinations and quantification of different analytes, especially concerned with the use of polymers as agglutinants, such as epoxy [4–6], polyester [7], PVC [8] and polypyrrole [9,10]. This type of solid composite graphite electrodes exhibit several important properties, such as polishing surface regeneration, rigidity, easiness of fabrication, economy and possibility of using in nonaqueous solvents.

The use of a carbon composite material prepared from castor oil derivative polyurethane and graphite as an electrode material has been proposed [11–15]. The graphite–polyurethane composite presents a number of important advantages, such as reduced risk to the environment since the vegetable oil is a renewable raw material, low temperature in the curing process, easiness of preparation by simply mixing the polyurethane binder with carbon and eventual modifiers, high hydrophobicity and resistance to many nonaqueous solvents, acid and basic solutions. In addition, the hydrophobic character of the polyurethane resin also prevents the swelling effect observed for epoxy resins composites when electrodes are used in aqueous media.

Atomic force microscopy (AFM) is a powerful and versatile technique for imaging surface topography, offering the unique possibility to quantify the roughness of the surface at a nanometer level with high resolution. AFM allows imaging in ambient conditions without any additional sample preparation such as gold coating as required for scanning electron microscopy, which makes it an ideal technique for the investigation of the effect of surface roughness of carbon composite electrodes.

* Corresponding author.
E-mail address: brett@ci.uc.pt (A.M. Oliveira Brett).

http://dx.doi.org/10.1016/j.jelechem.2014.07.027
1572-6657/

The aim of this work was to perform an AFM study to enable the understanding of the electrode surface morphology of composite electrodes prepared by graphite agglutinated by castor oil derivative polyurethane at the nanometer level, and the electrochemical characterisation by cyclic voltammetry and electrochemical impedance spectroscopy of the electron transfer processes at the graphite–polyurethane composite electrode surface. Systematic AFM and electrochemical studies of different weight percentages of graphite, 30–70% graphite w w^{-1}, in the graphite–polyurethane composites electrodes were carried out.

2. Experimental

2.1. Materials and reagents

Solutions of potassium ferrocyanide $K_4Fe(CN)_6$ from Merck were prepared in 0.1 M phosphate buffer in pH = 7.0 electrolyte solution. All experiments were done at room temperature (25 ± 1 °C). All solutions were prepared using analytical grade reagents and purified water from a Millipore Milli-Q system (conductivity $\leqslant$ 0.1 μS cm^{-1}).

2.2. Graphite–polyurethane composite preparation

The electrodes were prepared using different weight percentages of graphite, 30–70% graphite–polyurethane w w^{-1} [11,12].

The castor oil derivative polyurethane resin (POLIQUIL Brazil) was prepared by mixing 0.85 parts of the pre-polymer (A-249) and 1.0 part of the polyol (B-471) (w w^{-1}), according to the manufacturer instructions.

The polyurethane resin was mixed with < 20 μm diameter graphite powder (Aldrich, USA) in order to obtain 30%, 40%, 50%, 60% and 70% graphite–polyurethane w w^{-1} in the composite. The graphite–polyurethane composites were inserted in a hand press and extruded as rods with 3 mm diameter and cut in 1.5 cm long pieces.

All the graphite–polyurethane composite electrodes were polished in a 600 grit sand paper and again with γ-Al_2O_3 (1 μm) suspension with an APL-2 polishing wheel (Arotec, Brazil), and sonicated in water followed by isopropyl alcohol, five minutes in each solvent.

2.3. Atomic force microscopy characterisation

The surface morphological characterisation of graphite–polyurethane composites was performed using contact mode AFM in air. AFM was performed with a PicoSPM interfaced with a PicoScan controller (Agilent Technologies, USA). All the AFM experiments were performed with an AFM scanner with a scan range of 80 μm in *x*–*y* (Agilent Technologies, USA). Silicon nitride probes, V shaped cantilever configuration, of 200 μm length and 0.12 N m^{-1} spring constant (Agilent Technologies, USA) were used. All AFM images were taken with 256 samples/line *x* 256 lines and scan rates of 0.8–2.0 lines s^{-1}. When necessary, in order to remove the background slope the AFM images were processed by flattening, and the contrast and brightness were adjusted.

Section analyses were performed with PicoScan software version 5.3.3 (Agilent Technologies, USA). The roughness measurements were performed over the entire scan area of 3 μm × 3 μm and 1 μm × 1 μm scan-size images, using the PicoScan software version 5.3.3 (Agilent Technologies, USA).

The root mean square (*r.m.s.*) roughness represents the standard deviation of the heights in the topographical image and was calculated by:

$$r.m.s.\ \text{roughness} = \sqrt{\frac{1}{n-1}\sum_{selection}(Z_i - Z_{average})^2} \tag{2.1}$$

where Z_i is the height value at the *i* point in the image, *n* is the number of points in the image and $Z_{average}$ is the average height calculated by:

$$z_{average} = \frac{1}{n}\sum_{selection} z_i \tag{2.2}$$

The *r.m.s.* roughness mean values and the standard deviations presented in the paper were calculated using different AFM images taken at different locations on the surface of the polyurethane and graphite–polyurethane composite electrodes.

2.4. Cyclic voltammetry and electrochemical impedance spectroscopy

The voltammetric experiments were carried out using an Ivium CompactStat running with Ivium software (Ivium Technologies, The Netherlands). A system of three electrodes was used, which consisted of an SCE as reference electrode, a platinum wire as auxiliary and graphite–polyurethane composite working electrodes prepared as described in Section 2.5. All electrochemical measurements were performed in a Faraday cage. Cyclic voltammograms (CVs) were recorded at different scan rates using a 2 mV step potential and scan rate 100 mV s^{-1}.

The electrochemical impedance spectroscopy (EIS) measurements were carried out using a perturbation of 10 mV. The data was collected for 58 harmonic frequencies from 50 kHz to 0.1 Hz, at 10 steps/decade, and different polarisation potentials: +0.00 V, +0.21 V and +0.40 V vs. SCE. The impedance spectra were analysed by fitting to a Randles-type equivalent electrical circuit using ZView software (Scribner Associates, USA), Scheme 1.

The R_Ω is composed of the solution and the bulk composite resistances.

The constant phase elements, defined as:

$$CPE = -(Ci\omega)^{-\alpha} \tag{2.3}$$

is modelled as a non-ideal capacitor where the capacitance *C* describes the charge separation at the double layer interface and the α exponent is due to the heterogeneity of the surface.

The R_{ct} is the charge-transfer resistance.

The definition of the Warburg element used is:

$$Z_W(W_O) = R_{diff}(i\tau\omega)^{-\alpha}\text{ctnh}([i\tau\omega]^{\alpha}) \tag{2.4}$$

where R_{diff} is a diffusion resistance of electroactive species, τ is a time constant depending on the diffusion rate ($\tau = l^2/D$, where *l* is the effective diffusion thickness, and *D* is the effective diffusion coefficient of the specie), and $\alpha = 0.50$ for a perfect uniform flat interface.

Values of α less than 0.50 correspond to a not uniform interface (as happens with *CPE* non-ideal capacitance when $\alpha < 1$).

2.5. Graphite–polyurethane composite electrode

The graphite–polyurethane composite electrodes, used in the voltammetric experiments, were prepared gluing with silver epoxy

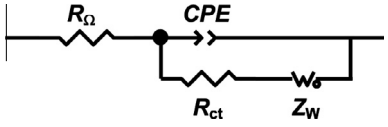

Scheme 1. Model circuit for EIS data fitting.

a conductive wire to the graphite–polyurethane sample. After drying, the contact was isolated with epoxy resin.

The graphite–polyurethane composite working electrodes were polished using diamond (particle size 1 μm) (Kemet Int., UK) before each electrochemical experiment. After polishing, they were rinsed thoroughly with Milli-Q water. Following this mechanical treatment, the electrode was placed in a buffer supporting electrolyte and voltammograms were recorded until a steady state baseline voltammogram was obtained. This procedure ensured very reproducible experimental results.

3. Results and discussions

3.1. Atomic force microscopy characterisation

The surface morphology of the graphite–polyurethane composite electrodes influenced their electrochemical properties, and was investigated by AFM in air. The AFM topographic images provided information on the roughness of the electrode surface and on the dimensions of the graphite particles. For the *r.m.s.* roughness statistics, different AFM images taken at different locations on

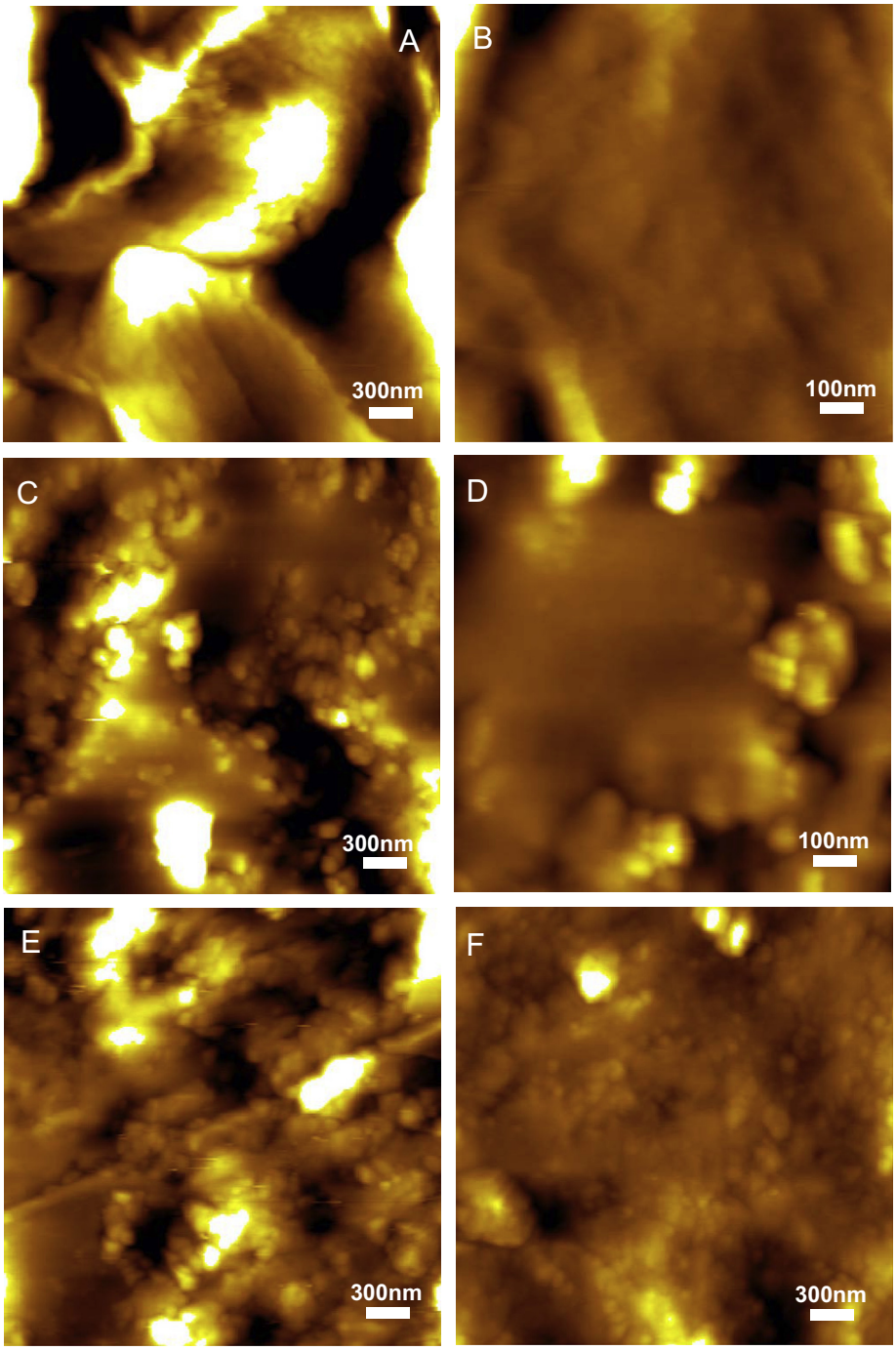

Fig. 1. AFM topographical images: (A and B) polyurethane and (C–F) graphite–polyurethane composite electrode surfaces: (C and D) 30%, (E) 40% and (F) 50% graphite–polyurethane w w^{-1}. (A, C, E, F) scan-size 3 μm × 3 μm, *z* range 120 nm, and (B and D) scan-size 1 μm × 1 μm, *z* range 50 nm.

the surface of polyurethane, and of the graphite–polyurethane composite electrodes, were used.

The castor oil derivative polyurethane resin morphological characteristics were studied and the results were essential to explain the composite characteristics after the incorporation of graphite particles into the polyurethane resin. The polyurethane resin surface images of 3 μm × 3 μm scan-size showed the occurrence of very large peaks and valleys, the images presenting an *r.m.s.* roughness of 192.90 ± 25.74 nm, Eq. (2.1), Fig. 1A. However, higher magnification images obtained on the lateral sides of the peaks revealed a very smooth morphology with *r.m.s.* roughness of only 26.1 0 ± 3.34 nm, as observed in the 1 μm × 1 μm size images, Fig. 1B.

The incorporation of the graphite powder into the polyurethane resin modified the morphological characteristics of the polyurethane surface.

AFM images of the graphite–polyurethane composite surface obtained after mixing a small percentage of graphite powder, 30% graphite–polyurethane w w^{-1}, into the polyurethane matrix, presented a much smoother surface of 61.30 ± 8.99 nm *r.m.s.* roughness, 3 μm × 3 μm scan-size, Fig. 1C, when compared with the polyurethane resin, Fig. 1A. However, the graphite–polyurethane

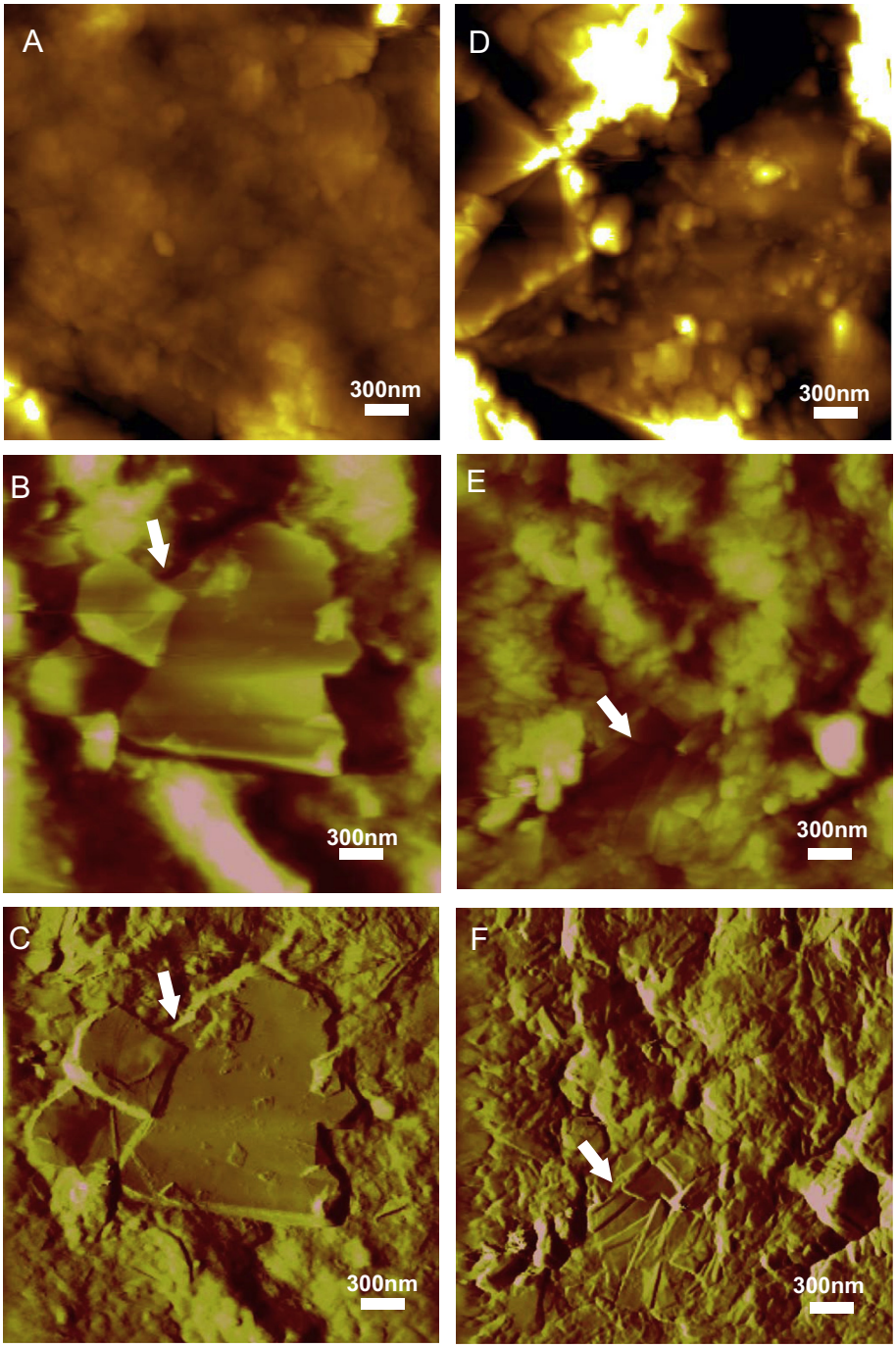

Fig. 2. AFM images of graphite–polyurethane composite electrode surfaces: (A–C) 60% and (D–F) 70% graphite–polyurethane w w^{-1}; (A, B, D, E) topographical, scan-size 3 μm × 3 μm, *z* range 120 nm and (C and F) deflection images, scan-size 3 μm × 3 μm, *z* range 0.5 nm.

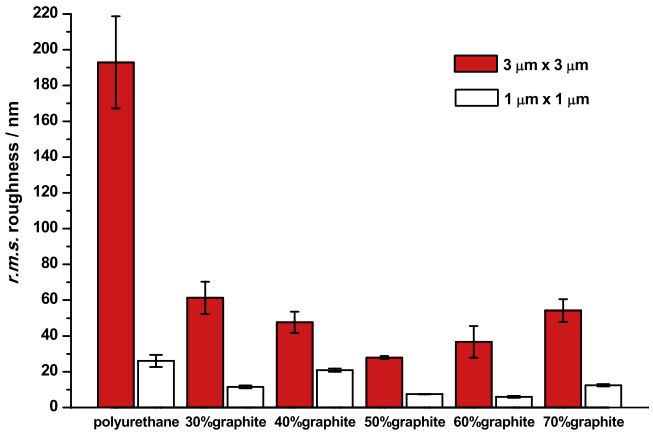

Fig. 3. Histogram of the *r.m.s.* roughness of polyurethane and graphite–polyurethane composite surfaces generated with the values measured in the AFM images of scan-sizes: (■) 3 μm × 3 μm and (□) 1 μm × 1 μm.

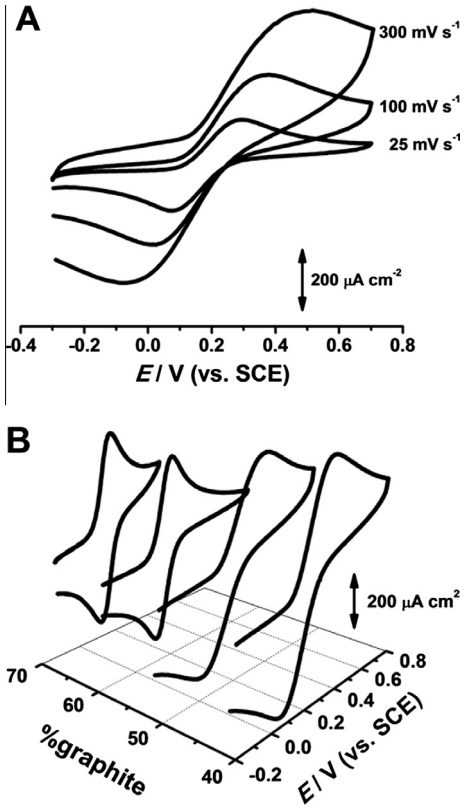

Fig. 4. CVs in 1 mM $K_4Fe(CN)_6$ in 0.1 M phosphate buffer pH = 7.0, at v = 100 mV s^{-1}: (A) 50% graphite–polyurethane w w^{-1} composite at different scan rates and (B) 3D plot of different percentages graphite–polyurethane composite electrodes.

composite morphology was very inhomogeneous, showing the occurrence of small aggregates 30–200 nm in diameter, which was better observed in the higher magnification image, Fig. 1D. The 30% graphite–polyurethane w w^{-1} composite surface, at the 1 μm × 1 μm scan-size, also presented a smaller *r.m.s.* roughness of 11.58 ± 0.78 nm, when compared with the same scan-size image for polyurethane, Fig. 1B. The morphology observed for the 30% graphite–polyurethane w w^{-1} composite was mainly due to a re-organisation of the polyurethane resin morphology in the presence of the graphite powder, since the 1–2 μm graphite particles diameter were only very rarely observed in the images.

The AFM images of the graphite–polyurethane composite surface obtained with larger weight percentages of graphite powder showed areas with only polyurethane, as well as areas of polyurethane resin with embedded graphite particles.

The AFM images of the graphite–polyurethane composites obtained with 40%, Fig. 1E, 50%, Fig. 1F, and 60%, Fig. 2A, graphite–polyurethane w w^{-1}, also showed large areas where only the polyurethane resin was present, with a surface morphology similar to that obtained for the 30% graphite–polyurethane w w^{-1} composite electrode, Fig. 1C, formed by aggregates of 30–200 nm of diameter. The *r.m.s.* roughness measured in the 3 μm × 3 μm scan-size images was: 47.67 ± 5.95 nm for 40%, 27.9 0 ± 0.85 nm for 50% and 36.72 ± 8.8 nm for 60% graphite–polyurethane w w^{-1}. Higher magnification AFM images of 1 μm × 1 μm scan-size also presented areas with similar morphologies to the 30% graphite–polyurethane w w^{-1} composite, and the *r.m.s.* roughness values measured were: 20.85 ± 0.92 nm for 40%, 7.46 ± 0.01 nm for 50% and 5.97 ± 0.47 nm for 60% graphite–polyurethane w w^{-1}, consistent with the rearrangement of the polyurethane matrix in the presence of graphite powder.

For the graphite–polyurethane composite containing 70% graphite–polyurethane w w^{-1}, areas containing only polyurethane resin, without the presence of graphite particles, 3 μm × 3 μm scan-size images, were observed very rarely, Fig. 2D and E. The *r.m.s.* roughness measured in the 3 μm × 3 μm size images increased slightly to 54.23 ± 6.36 nm, due to the presence of these graphite particles. Nevertheless, the *r.m.s.* roughness measured in small, 1 μm × 1 μm scan-size images, containing manly the polyurethane matrix, was 12.4 ± 0.64 nm, demonstrating the same rearrangement of the polyurethane in the presence of graphite.

For all graphite powder weight percentages, sporadically graphite fragments and/or particles (marked with white arrows) could be observed in the AFM topographical images for 60% graphite–polyurethane w w^{-1}, Fig. 2B, and for 70% graphite–polyurethane w w^{-1} composites, Fig. 2D and E. The atomically smooth graphite basal planes and the sharp layered edges of the graphite nanosheets observed in the topographical images, Fig. 2B and E, are even more evident in the deflection images, Fig. 2C and F, acquired simultaneously with the topographical ones.

The *r.m.s.* roughness calculations obtained for large 10 μm × 10 μm scan scale AFM images of the graphite–polyurethane composite electrodes showed similar results, not dependent

Table 1
Graphite–polyurethane composite electrodes: current ratio, potential difference, potential variation with log v, charge transfer coefficient, current variation with $v^{1/2}$ and electrode area from CVs in $K_4Fe(CN)_6$ in 0.1 M phosphate buffer pH = 7.0.

Graphite–polyurethane (% w w^{-1})	I_{pa}/I_{pc}	ΔE_p (mV)	$E_p - E_{p/2}$ (mV)	α	$dI_{pa}/d(v^{1/2})$ A/$V^{1/2}$ $s^{-1/2}$	A (cm^2)
40	1.23	223	290	0.16	–	0.016[a]
50	1.12	210	230	0.21	2.8×10^{-5}	0.025
60	1.01	200	130	0.36	1.8×10^{-4}	0.146
70	1.06	186	96	0.49	5.9×10^{-5}	0.053

[a] The electrode area was estimated from the currents registered at v = 50 mV s^{-1}.

on the weight percentage of graphite powder incorporated into the resin. Indeed, the AFM images of the polyurethane resin with embedded graphite powder showed similar morphologies, with parallel lines separation caused by the polishing process with 1 μm diameter γ-Al_2O_3 particles.

Taking into consideration all the AFM results obtained for polyurethane resin and graphite–polyurethane composite surfaces, it can be concluded that the *r.m.s.* roughness of the polyurethane decreased drastically after the incorporation of the graphite powder, as can be observed in the histogram, Fig. 3. This is due to a decrease of the polyurethane hardness after the mixture with soft graphite particles, the composite surface being easily and smoothly polished. The smoother graphite–polyurethane surfaces were obtained for 50–60% graphite–polyurethane w w^{-1}.

3.2. Electrochemical characterisation

3.2.1. Cyclic voltammetry

CVs were obtained with all graphite–polyurethane composite electrodes for different scan rates in solutions of 1 mM $K_4Fe(CN)_6$ in 0.1 M phosphate buffer pH = 7.0.

The 30% graphite–polyurethane w w^{-1} electrode did not show any electrochemical response due to a high ohmic resistance. The ohmic resistance decreased suddenly from ~30 MΩ, in the case of 30% graphite–polyurethane w w^{-1}, down to 35 Ω for the 70% graphite–polyurethane w w^{-1}, in agreement with CVs results [11]. The oxidation and the reduction peak potentials were slightly shifted to more positive and more negative potentials, with increasing scan rate, Fig. 4A.

Also, the peak width decreased with increasing graphite percentage. From the relationship:

$$|E_p - E_{p/2}| = 47.7(\alpha n')^{-1} \quad (3.1)$$

where α is the charge transfer coefficient and n' the number of electrons transferred in the rate-determining step, and considering $n' = 1$, the charge transfer coefficient α, calculated for each graphite–polyurethane composite electrode, increased with increasing graphite/polyurethane ratio.

Increasing the scan rate the peak current increased linearly with the square root of v, consistent with the diffusion-limited redox reaction. The peak current in amperes for a diffusion-controlled irreversible system is given by:

$$I_p/A = \pm 0.4463(F^3/RT)^{1/2} n(\alpha n')^{1/2} A D^{1/2} C v^{1/2} \quad (3.2)$$

where the positive sign is for anodic and negative for cathodic redox reaction. In Eq. (3.2), n is the number of electrons transferred during the redox reaction, A is the electrode area in cm^2, D is the diffusion coefficient in $cm^2\ s^{-1}$, C is the concentration in mol cm^{-3} and v is in V s^{-1} [2]. For $T = 298$ K, the term 0.4463 $(F^3/RT)^{1/2} = 2.69 \times 105$ A s/mol $V^{1/2}$. Considering that $n = 1$, and plotting I_p vs. $v^{1/2}$, the A for different percentages graphite–polyurethane composite electrodes was obtained, Table 1. For this calculation, the diffusion coefficient of $Fe(CN)_6^{4-}$, in 0.1 M phosphate buffer pH = 7.0, was $D = 7.35 \times 10^{-6}\ cm^2\ s^{-1}$.

The anodic and cathodic currents ratio for each electrode decreased with increasing graphite percentage, Table 1. Also, increasing the graphite/polyurethane ratio the oxidation and reduction peaks shifted to less positive and negative values, respectively, Fig. 4B. Thus, the peak potential difference between the oxidation and the reduction peaks decreased in agreement with the increase of the system reversibility for higher graphite–polyurethane ratio.

Voltammetric results obtained with graphite–castor oil polyurethane composite electrode demonstrated that the 60% graphite–polyurethane w w^{-1} presented better reproducibility, mechanical and electric resistance, easy preparation and surface

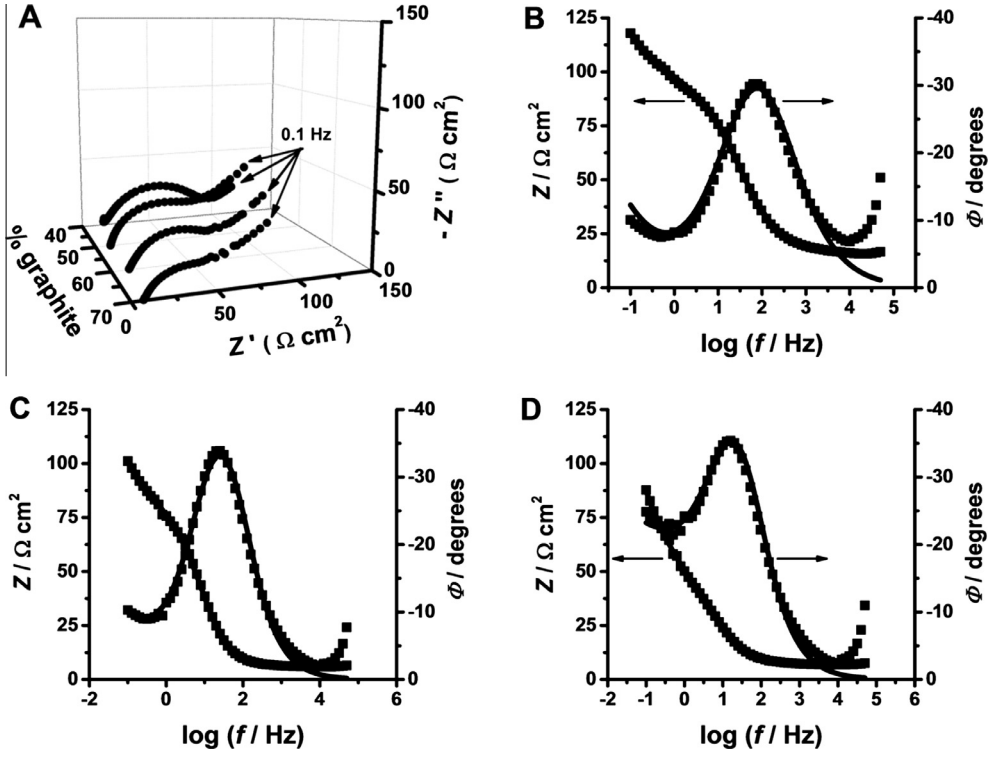

Fig. 5. EIS in 3 mM $K_4Fe(CN)_6$ at +0.21 V in 0.1 M phosphate buffer pH = 7.0: (A) 3D plot of the complex plane representation at different percentages graphite–polyurethane composite electrodes, and (B–D) total impedance (●) Z and phase angle (■) Φ variation with frequency f: (B) 40%, (C) 60% and (D) 70% graphite–polyurethane w w^{-1} composite electrodes.

Table 2
Graphite–polyurethane composite electrodes: EIS data fitting equivalent circuit (Scheme 1, Fig. 5). Spectra recorded at +0.21 V vs. SCE in 3.00 mM $K_4Fe(CN)_6$ in 0.1 M phosphate buffer pH = 7.0.

Graphite–polyurethane (%)	R_Ω (Ω cm^2)	*CPE*		R_{ct} (Ω cm^2)	Z_W		
		C (F cm^{-2})	α		R_{diff} (Ω cm^2)	τ (s)	α
40	10.2	5.6×10^{-4}	0.73	75.4	0.3	0.0009	0.27
50	6.1	8.2×10^{-4}	0.76	61.1	0.8	0.0009	0.25
60	7.5	9.3×10^{-4}	0.78	53.8	1.1	0.0010	0.24
70	7.2	1.4×10^{-3}	0.80	30.7	2.4	0.0010	0.21

renovation [11], and the results for the graphite–epoxy composite electrodes showed the best electroanalytical properties for the 60% graphite–epoxy composition [6].

3.2.2. Electrochemical impedance spectroscopy

Electrochemical impedance spectra (EIS) in 3 mM $K_4Fe(CN)_6$, in 0.1 M phosphate buffer pH = 7.0, at +0.21 V fixed potential vs. SCE, which is close to the open circuit potential value ~0.20 V, were recorded, Fig. 5A.

The EIS obtained always included two regions: a semi-circular part at high frequencies corresponding to the electron transfer process and a linear part at lower frequencies corresponding to diffusion, Fig. 5A, and EIS showed that, increasing the graphite–polyurethane percentage, both real and imaginary impedance decreased.

The EIS were fitted, Fig. 5B–D, using a Randles-type equivalent electrical circuit, Scheme 1, formed by the electrochemical cell resistance, R_Ω, and a parallel combination of a constant phase element, *CPE*, Eq. (2.3), representing the interfacial capacitance, the charge transfer resistance, R_{ct}, and a Warburg element, Z_W, Eq. (2.4), simulating the diffusion process.

Data from analysis of EIS, Table 2, showed the R_{ct} decrease in agreement with the increase of conductivity upon greater incorporation of graphite powder into the polyurethane matrix. The cell resistance, R_Ω, showed small fluctuations with values between 10 and 6 Ω cm^2. Also, the interfacial capacitance, C, increased with graphite percentage due to an increase of the electroactive surface area per cm^2 and the formation of a more compact double-layer, whereas the increase of the heterogeneity parameter, α, is in agreement with the AFM results which show that the roughness of the polyurethane decreased after the incorporation of the graphite powder, Fig. 3.

The smoother graphite–polyurethane surfaces were obtained for 60% graphite–polyurethane w w^{-1}. The diffusion resistance increased with the graphite powder incorporation, in agreement with the increase of the interfacial capacitance, due to the difficulty of the $Fe(CN)_6^{4-}$ ions to diffuse through a more compact double-layer. Also, the electrode roughness is responsible for the capacitance and consequently for the diffusion resistance changes, since the surface is not uniformly accessible to mass-transfer. However, the diffusion process time constant magnitude was maintained.

4. Conclusions

The morphology of graphite–castor oil polyurethane composite electrodes with different weight percentages of graphite, 30–70% graphite–polyurethane w w^{-1}, was investigated by AFM, and voltammetry.

The AFM images and the *r.m.s.* roughness measurements demonstrated that the polyurethane roughness decreased with increasing the graphite content, for 3 μm × 3 μm and 1 μm × 1 μm scan-size images. The 50% and 60% graphite–polyurethane w w^{-1} composites presented smoother surfaces. Increasing the graphite–polyurethane content to 70% increased the roughness of the electrode surfaces.

The electrochemical characterisation of the graphite–castor oil polyurethane composite electrodes was performed in solutions of $K_4Fe(CN)_6$ by CV and EIS. The CV showed that the potential difference between the oxidation and the reduction peaks decreased with increasing graphite–polyurethane ratio. A better peak resolution was observed for the electrode containing 60% graphite–polyurethane w w^{-1}. The EIS spectra charge transfer resistance significant decrease with increasing the graphite content, and the capacitance increase due to an increase in the electroactive area of the electrode, was observed.

The AFM and voltammetric results enabled the conclusion that the 60% graphite–polyurethane w w^{-1} was the optimal composition for preparation of the graphite–castor oil polyurethane composite electrodes.

Conflict of Interest

The authors confirm that there is no conflict of interest.

Acknowledgments

Financial support from: Fundação para a Ciência e Tecnologia (FCT), Projects PTDC/QEQ-MED/0586/2012, PTDC/DTP-FTO/0191/2012, PTDC/SAU-BMA/118531/2010, PEst-C/EME/UI0285/2013 and CENTRO-07-0224-FEDER-002001 (MT4MOBI)(co-financed by the European Community Fund FEDER), FEDER funds through the program COMPETE – Programa Operacional Factores de Competitividade as well as CAPES-FCT 177/07 and FAPESP 11080-7, is gratefully acknowledged.

References

[1] J. Wang, Analytical Electrochemistry, Second ed., Wiley VCH Publishers, New York, 2000, pp. 113–116.
[2] C.M.A. Brett, A.M. Oliveira-Brett, Electrochemistry: Principles, Methods and Applications, Oxford Science Publications, Oxford, 1993.
[3] D. O' Hare, J.V. Macpherson, A. Willows, Electrochem. Commun. 4 (2002) 245–250.
[4] L. Moreno-Baron, A. Merkoçi, S. Alegret, Electrochim. Acta 48 (2003) 2599–2605.
[5] A. Doménecha, J. Alarcón, Anal. Chim. Acta 452 (2002) 11–22.
[6] J. Navarro-Laboulais, J. Trijueque, F. Vicente, H. Scholl, J. Electroanal. Chem. 379 (1994) 159–163.
[7] A. Doménech-Carbó, M.T. Doménech-Carbó, L. Osete-Cortina, J.V. Gimeno-Adelantado, F. Bosch-Reig, R. Mateo-Castro, Talanta 56 (2002) 161–174.
[8] F. Albertús, A. Llerena, J. Alpízar, V. Cerdá, M. Luque, A. Ríos, M. Valcárcel, Anal. Chim. Acta 355 (1997) 23–32.
[9] J.H. Park, J.M. Ko, O.O. Park, D.W. Kim, J. Power Sources 105 (2002) 20–25.
[10] H.Y. Lee, J.Y. Kim, J.H. Park, Y.G. Joe, T.H. Lee, J. Power Sources 131 (2004) 188–193.
[11] R.K. Mendes, S. Claro-Neto, E.T.G. Cavalheiro, Talanta 57 (2002) 909–917.
[12] C.M.F. Calixto, R.K. Mendes, A.C. Oliveira, L.A. Ramos, P. Cervini, E.T.G. Cavalheiro, Mater. Res. 10 (2007) 109–114.
[13] R.K. Mendes, P. Cervini, E.T.G. Cavalheiro, Talanta 68 (2006) 708–712.
[14] P. Cervini, L.A. Ramos, E.T.G. Cavalheiro, Talanta 72 (2007) 206–209.
[15] R.A. de Toledo, C.M.P. Vaz, Microchem. J. 86 (2007) 161–165.